A Series Elastic Composite Actuator for Soft Arm Exosuits

Design and Preliminary Test

Leonardo Cappello
Dept. of Robotics, Brain
and Cognitive Sciences
Istituto Italiano di Tecnologia
Genova, Italy
Email: leonardo.cappello@iit.it

Alberto Pirrera
and Paul Weaver
Advanced Composites Ctre
for Innovation & Science
University of Bristol
Bristol, UK

Lorenzo Masia
School of Mechanical
& Aerospace Engineering
Nanyang Technological University
Singapore
Email: lorenzo.masia@ntu.edu.sg

***Abstract*—The paper introduces a novel type of actuator for soft wearable exoskeletons providing assistance to the elbow joint motion. The mechanism consists of two DC motors, a multistable composite transmission which introduces series elastic properties, a high-efficiency non-backdrivable mechanism and a pair of Bowden cables to transmit the motion from the actuator to the joint. A test bench has been designed to experimentally characterize the performance of the proposed device. The control architecture is then introduced and described. The results of preliminary tests are shown and discussed. In conclusion, future developments and a embodiment of the envisioned application are introduced.**

I. Introduction

The development of robotic wearable devices for human assistance is relatively longstanding in the field of robotics and their impact is increasing in recent years [1]–[4] . This class comprises rigid exoskeletons and soft exosuits which applications range from teleoperation to locomotion support and object handling. Several American, European and Asian research programs are boosting the research in this field and a considerable number of active exoskeletons and soft suites are being developed and tested worldwide. Such technologies are meant to be used in parallel with the users body to empower or replace the functionality of the limbs. Belonging to this class of devices, soft exosuits are systems which exploit users joints rather than providing rigid articulated links and kinematics [5]. They are usually cable driven and based on textile supports. The actuators are relocated with respect to the joints, e.g. on the torso of the wearer, so that the only added weight on the limb is the one of the cables and the textiles. This family of exoskeletons, which could be more properly considered exomuscles, introduce a number of advantages with respect to the rigid exoskeletons [7] they are lightweight, allow easy adjustment and alignment, have low inertia and low profile and introduce little to no effect on kinematics. However, intrinsic limitations comprise: low to medium bandwidth due to the compliant suite and human interface, lower disposable torques and only tensile forces applicable due to the cable driven actuation (since that a cable can only pull and not push). Despite the theoretical advantages, to date this discipline requires innovations in several fields before to provide fully functional prototypes. Actuation design is one of the most crucial factor of the design for several reasons: an effective actuation indeed could provide significant advantages in terms of interaction safety, power efficiency and ergonomics. To obtain this outcomes we introduce the design of a functional actuator that merges traditional electromechanical motors and a multistable composite structure previously developed by the authors [8]–[10]. Such structure, made of carbon fibre flanges and metal parts, introduces a serial non-linear elastic behavior. Furthermore the composite material structures allow to have multiple points of local stability in the workspace: i.e. multistability. Hence when smartly designed and controlled, the fact of having multiple point of equilibrium in the compliant structure, results in increased power efficiency. In this preliminary work, we present an actuator which has been designed to assist the elbow motion and meant to be used in a soft wearable arm exoskeleton currently under development which exploits principles similar to [11]. In the following sections the design process and experimental results are discussed.

II. Design

A. Requirements

The actuator should weigh less than 2 kg and be smaller than 400 x 200 x 200 mm to be mounted on the torso of a wearable exoskeleton. Considering the application, the maximum torque that the actuator should generate at the joint level should be enough to lift the forearm and a load carried by the hand. Accordingly to figure 1, the maximum torque that the system has to sustain is:

$$C_{max} = W_{arm} \cdot L_{cfa} + W_{load} \cdot L_{fa} \tag{1}$$

considering an average weight of the forearm W_{arm} of 20 N, an average position of the center of mass of the forearm L_{cfa} equal to 150 mm far from the elbow joint, an average length of the forearm L_{fa} of 300 mm [12] and a load W_{load} of 10 N on the hand.

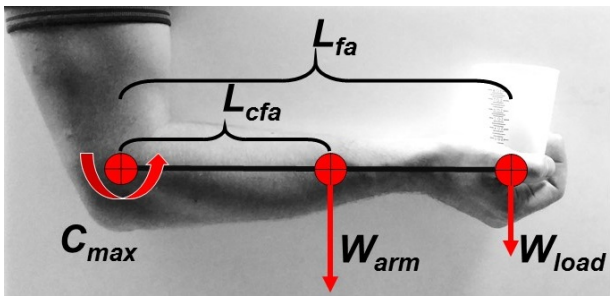

Fig. 1. Representation of the loads acting on the elbow joint.

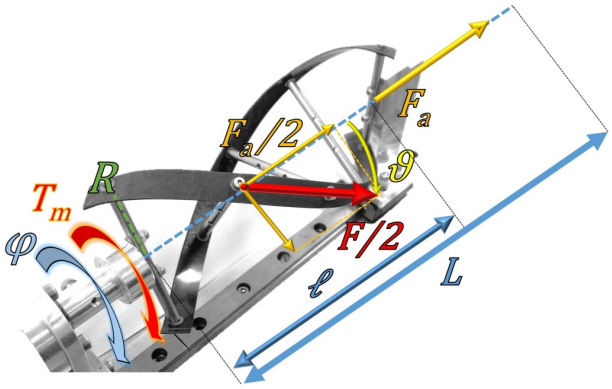

Fig. 2. The MCT transmission depends on the twisting angle of the structure. Only the partially coiled configuration of length ℓ is displayed, while the totally uncoiled configuration is long L.

To ensure an intrinsic safe interaction with the user, to avoid breakage when unpredicted contacts occur and to implement energy storage the transmission is provided with a non-conventional serial elastic element [13], [14].

B. The multistable composite transmission

To develop the desired elasticity, therefore, the Multistable Composite Transmission (MCT) [8]–[10] has been incorporated in the design. Such transmission consists of two pre-stressed flanges of carbon fibres held together by metal connecting spokes as shown in figure 2. The structure is able to twist and take any configuration between a coiled and a straight shape. If one end of the structure is constrained to translate and not to rotate, and a torque is applied on the other end, the overall structure twists depending on the rotation impressed. The torque of the motor is hence translated into an axial force that depends on the twisting angle of the structure [9]. According to figure 2, the axial force transmitted is equal to:

$$F_a = \frac{T_m}{R} \cdot \frac{\cos(\theta)}{\sin(\theta)} \tag{2}$$

and given that [8]

$$\theta = \sin^{-1}(\frac{R \cdot \phi}{L}); \tag{3}$$

$$F_a = \frac{T_m}{R} \cdot \cot(\sin^{-1}(\frac{R \cdot \phi}{L})) \tag{4}$$

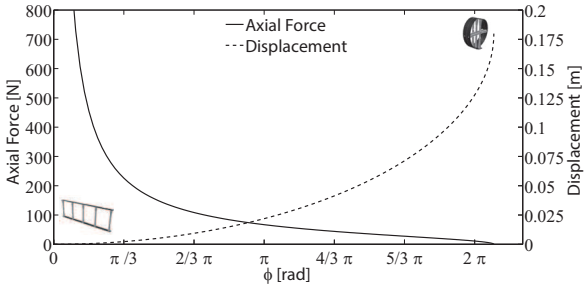

Fig. 3. Resulting axial force (solid) when a torque of 1 Nm is applied at one end of the MCT and relative axial displacement of the structure (dashed) as function of the twisting angle ϕ.

From this point onwards the straight (completely extended) configuration will be referred as the reference one, corresponding to the origin and twist angle equal zero. The axial displacement of one end of the structure is [8]

$$\Delta\ell = L - \ell = L \cdot (1 - \cos(\theta)) = L \cdot (1 - \cos(\sin^{-1}(\frac{R \cdot \phi}{L}))) \tag{5}$$

Plots of the theoretical axial force and linear displacement are reported in figure 3, where geometrical dimensions of table I are used and a unitary torque applied. Only half of the total range of ϕ is depicted since that it presents a symmetrical behavior with respect to the two possible coiling directions (one is obtained by twisting the helix counter-clockwise from the straight configuration, the other is obtained by twisting the helix clockwise). We will refer to them as direct coil (counter-clockwise twist) and inverse coil (clockwise twist).

The particular property of the MCT is the elastic energy profile depending on several design parameters previously studied by the authors [10]. To summarize, the main parameters influencing the energy profile of the structure are: the lay-up of the carbon fibre flanges, the angle β of the fibres (the lay-up is made of five layers of fibres oriented respectively at β, β, $0°$, β, β with respect to the main dimension of the flange), the length L, the radius R of the underlying cylinder, the width W of the flanges and the ratio α defined as:

$$\alpha = R_i/R \tag{6}$$

where R is the radius of the helix and R_i the manufacturing radius of the pre-stressed flanges produced on a cylindrical mould, hence α physically represents the amount of pre-stress. The particular set of parameters used for the experimental setup are reported in table I.

TABLE I. MCT PARAMETERS

Lay-Up	β	α	R	L	W
symmetric	45^o	2	27.4 mm	180 mm	10 mm

The strain energy curve [8] of the particular structure, in function of the angle ϕ applied at the extremity of the helix, is shown in figure 4 upper portion; in figure 4 lower portion

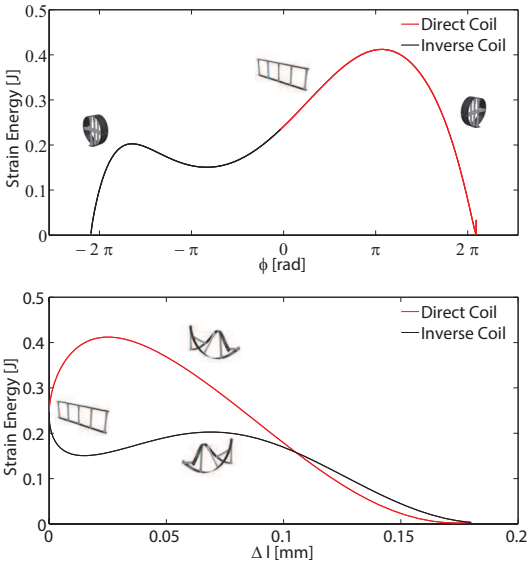

Fig. 4. Strain energy of the MCT as function of the twisting angle ϕ (upper portion). Strain energy of the MCT as function of the axial elongation $\Delta\ell$ (lower portion).

is instead represented the same strain energy with respect to the linear displacement. It must be noted that the strain energy is not symmetrical with respect to the two possible coiling directions due to the non symmetrical arrangements of the carbon fibre lay-up. The effect of the strain energy is a variable axial force generated by the structure itself which is summed to the one transmitted.

The points of maximum strain energy correspond to local unstable equilibria: if the system is in such configuration a perturbation makes it twisting towards one point of minimum energy; these points hence are stable equilibrium configurations corresponding to zero axial force and restoring force from the composite materials. The stable equilibria are used to display a behavior similar to a conventional (non-linear) serial spring connected to the motor while the unstable ones to store and release elastic energy.

C. Reconfiguring the MCT

To exploit the properties of the MCT, an additional actuator called reconfiguration actuator (ReAct) has been placed in series with the MCT in order to make each joint angle potentially correspond to each energy configuration of the multistable transmission. In other words the ReAct shifts the energy curve of the MCT with respect to the flexion angle of the actuated joint. Being the ReAct in series with the transmission the application differs from the macro-mini approach [6].

D. Overall design

The concept schematics of the actuator is shown in 5 upper portion. Space and weight constrains lead to a compact design for the proposed actuator as depicted in figure 5 lower portion. To actuate the helix a conventional electromechanical motor (motor 1 in figure 5, Maxon Ec-i 40, 70 W, 3.7:1

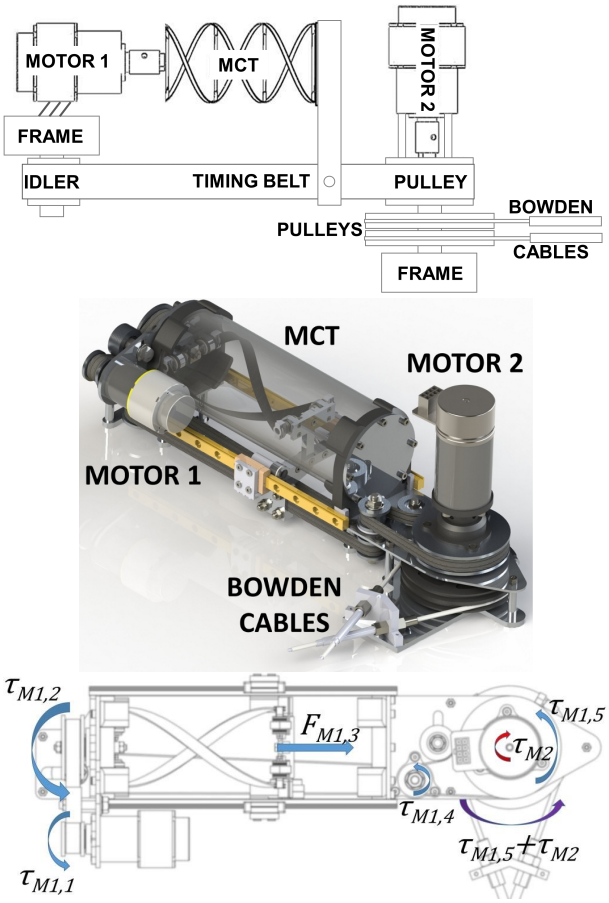

Fig. 5. Concept schematics (upper portion), CAD model (central portion) of the actuator. In the lower portion the top view of the prototype is shown where torque transmission is schematized. The torque generated by motor 1 ($\tau_{M1,1}$) is reduced ($\tau_{M1,2}$) and then converted into a force ($F_{M1,3}$) by the MCT. This force is converted into a torque ($\tau_{M1,4}$) by means of a timing belt and ulteriorly reduced ($\tau_{M1,5}$). It is finally summed with the torque generated by motor 2 (τ_{M2}). This torque is reduced again (not shown) by means of Bowden cables.

gearhead) is used whose motion is transferred through a timing belt coupling (reduction ratio 2:1) to the MCT. The MCT converts the rotational motion into a linear translation (reduction ratio equal to (5) expressed in mm/rad). The translating end of the MCT is thus connected to a timing belt which converts the translation again into a rotational motion (reduction ratio 19.10:2π $\approx$ 3:1 rad/mm). This motion is then transferred, through a timing belt coupling (reduction ratio 70.03:19.10 $\approx$ 3.67:1), to the body (stator) of the ReAct (motor 2 in figure 5, Maxon Ec45 flat, 70 W, 12:1 gearhead) which results in series with the first motor and rotates along its main axis. Finally the output shaft of the ReAct is connected to a pair of pulleys, each one pulling a Bowden cable (reduction ratio 7.7:1) connected to the joint in an agonist-antagonist configuration. The overall reduction ratio has been designed in order to make the helix elongation range of $\sim [0 \div 180]$ mm correspond to a joint angular range of $\sim [0 \div 120]^\circ$. The Bowden cables are then used to transfer the motion of the actuator with respect to the joint: the users limb is hence free from any bulky

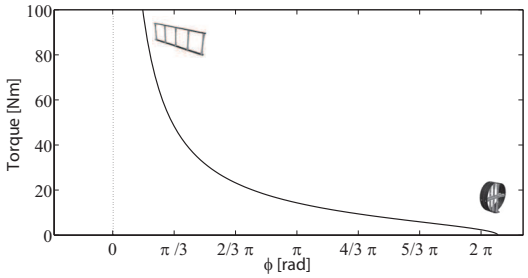

Fig. 6. Maximum static torque that the motor 1 can generate at the joint level as function of twisting angle ϕ. The dotted line represents the vertical asymptote.

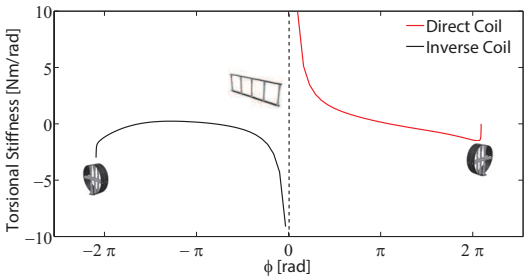

Fig. 7. Torsional stiffness of the MCT perceived at the joint level as function of the twisting angle ϕ. In red the direct coiling (obtained by twisting the MCT counter-clockwise), in black the inverse coiling (obtained by twisting the MCT clockwise).

component. The actuator itself will be placed on the back of the user and its weight carried by the users shoulders. Finally motors have been chosen in order to be able to apply at the joint level the required continuous torque of 6 Nm. As a result of the reduction, the maximum static torque that motor 1 can generate translated at the joint level is strictly not constant as depicted in figure 6 and depends on the angular configuration of the MCT. The MCT internal energy results in a passive torsional stiffness depending on the twist angle. Such stiffness, shown in figure 7, can be then actively adjusted at the control side. Differently from the torque transmitted, the torque generated by the MCT is not symmetrical with respect to the two coiling directions and hence they are both depicted. The ReAct is meant to reconfigure the transmission in order to save power, and this actuator is solely controlled actively when the reconfiguration of the MCT is needed. The motor is an EC brushless with a low reduction gearhead, chosen for its high power-to-weight ratio, and it is backdrivable. In order to experience compliancy at the joint level it is paramount that the load of the joint is transferred to the MCT and not to the shaft of the ReAct. To avoid undesired backdrivability of the ReAct which would result in a loss of elastic behavior a non-backdrivable mechanism (NBM) has been incorporated in the design. Such mechanism is coupled with the ReAct and embedded in the design. The use of traditional non-backdrivable systems like lead screw and worm gear pairs leads to low efficiency since that such non-backdrivability is due to the shear friction between the couplings. To avoid the introduction of low-efficiency transmissions, the NBM

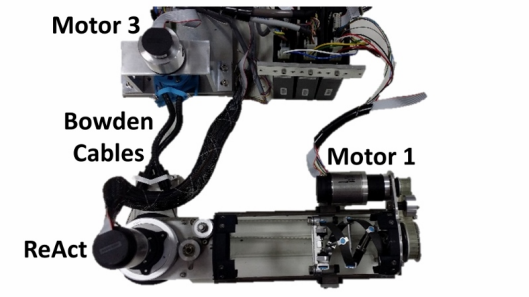

Fig. 8. Test bench comprising the actuator (lower portion) and the electrical motor used to simulate a load at the joint level (motor 3).

designed by Controzzi et al. [15] has been used. It is based on the wedge phenomenon and it allows a high-efficiency monodirectional transmission.

Finally, the Bowden cables will be routed through a soft wearable exoskeleton (currently in development) to act as an agonist-antagonist pair at the joint level. The dimensions of the actuator are 400 x 130 x 170 mm and the total weight is 1.8 kg : thus it can be carried as a backpack without excessive bulk and shoulder muscular effort.

III. Experimental Setup

A. Test bench

To perform preliminary tests and to validate the control architecture a test bench has been developed (figure 8). It comprises the physical model of the actuator remotely connected through a Bowden cables system (Igus® robolink®) and a pair of pulleys to another motor (Maxon Ec 45 flat, 70 W, direct drive) with the aim to simulate gravitational loads and to measure displacements at the joint level with the built-in encoder. The motors are driven by Maxon EPOS2 drivers (with internal PID controller whose gains selected with an auto-tuning procedure), the control code is written in Matlab® Simulink and interfaced with Quanser Quarc real-time control architecture.

B. Control model

The control scheme of the actuator, as depicted in figure 9, can be described as follows: corresponding to a desired angular joint position and a desired energy configuration, two motor displacements are computed, θ_{d1} for the motor 1 and θ_{d2} for the ReAct, piloted in torque through a PD controller ($K_{p1} + sK_{d1}$), displays a torque τ_{M1} to the MCT. The MCT converts the input torque to an output torque τ_T depending on the configuration of the helix. To this torque it is summed the elastic torque τ_E generated by the MCT itself, depending on the angular configuration. Finally the ReAct (motor 2), in series, generates a torque τ_{M2} which is subtracted to the one before the motor 2 resulting in a torque transmitted to the joint τ_R. This is possible by applying a relative motion θ_{MCT} which is reflected to the MCT structure. This relative motion affects both the torque transmitted and the one generated by the MCT. The ReAct is controlled in torque with a PD controller ($K_{p2} + sK_{d2}$).

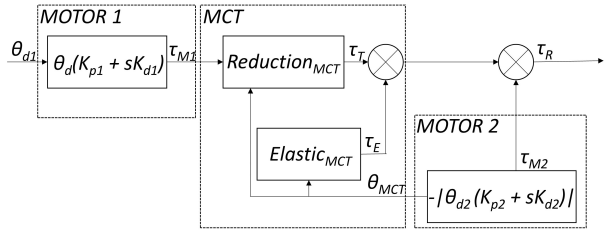

Fig. 9. Schematics of the control model, comprising the motor 1 controlled in torque with a proportional and derivative gain ($K_{p1}+sK_{d1}$). Such torque is transmitted by the MCT which also generate an elastic torque in addition. To such torque is subtracted the torque generated by motor 2, in series, controlled in torque with a proportional and derivative gain ($K_{p2}+sK_{d2}$). The torque is then transferred to the joint. The torque generated by motor 2 results in a twist of the MCT which affects both the torque transmission and the elastic torque generated.

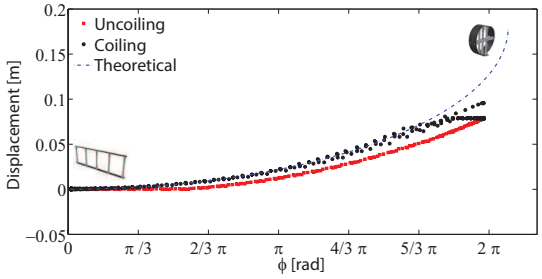

Fig. 10. Experimental values of coiling (in black) and uncoiling (in red) linear displacements with respect to the theoretical one (in blue) as function of the twisting angle ϕ.

By knowing the properties of the structure it is possible to handle the torque transmission/generation and thus save energy.

C. Transmission evaluation

To evaluate the performances of the transmission two different tests have been performed. First the non-linear reduction ratio of the MCT has been tested by applying a cyclic motion with the Motor 1 ranging from the totally extended helix configuration to the totally coiled one. Results are shown in figure 10 collected by means of the encoder of the motor 3. It is possible to see that the MCT coupled with the Bowden cable system introduces a hysteresis in the generated motion which slightly diverges from the theoretical one.

A second test has been performed to evaluate the total backlash generated by the NBM coupled with the Bowden cable system. A sinusoidal trajectory was impressed by the ReAct and the corresponding motion at the joint level was measured. Results are shown in figure 11. A total backlash of $\sim 8^\circ$ was measured.

D. Discrete motion application

To validate the effectiveness of the control architecture a discrete motion application paradigm has been tested. The concept is the following: starting from a stable equilibrium configuration, corresponding to a low stiffness (thus low

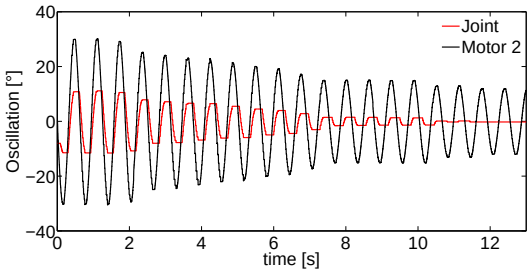

Fig. 11. Experimental determination of the total backlash. A sinusoidal motion is applied by motor 2 (in black), which is reflected to the joint and acquired by an encoder (in red). Corresponding to an oscillation of $\pm 8^\circ$ of ReAct, no motion is transferred to the joint.

elastic energy) and low transmission ratio of the MCT (coiled configuration), the system is reconfigured towards a higher stiffness (higher elastic energy) and transmission ratio in an unstable configuration. The configuration corresponds to a predefined desired joint angle. Once so reconfigured, the system is used to apply a motion. The higher transmission ratio and the release of the elastic energy increases the efficacy of the transmission. Once the motion is finished the system is again in a stable configuration. The three phases (reconfiguration, motion application and disabling motors), are described in details as follows and the corresponding motions are plot in figure 12.

- *Phase I*. Corresponding to the desired joint angle, the MCT angular displacement is computed. Since that the initial configuration of the helix corresponds to a point of minimum of the strain energy, the system is stable and the motor 1 is not draining current and is disabled on the motor driver. The motor is then enabled and controlled in torque to follow a minimum jerk trajectory to the desired angular value. Contemporarily the motor 2 (ReAct) is piloted to apply a contrary motion to hold the joint stationary. A minimum jerk motion law has been chosen in order to have a smooth trajectory with characteristics similar to the physiological voluntary motion [16], [17].
- *Phase II*. When the angular configuration is reached, the ReAct is disabled and motor 1 performs the same motion in the opposite direction. The result is hence a motion applied to the joint.
- *Phase III*. At the end of the motion the MCT will be in the stable equilibrium configuration: the motor 1 does not drain current and can be disabled. The system self-sustains in the new joint position and no active effort is required.

To summarize, from an initial position in which the system is stable, it moved to a final position and reconfigured itself in order to be stable again.

IV. Conclusions and Outlook

The proposed system combines a powerful transmission, a serial elastic element and a power-saving architecture in

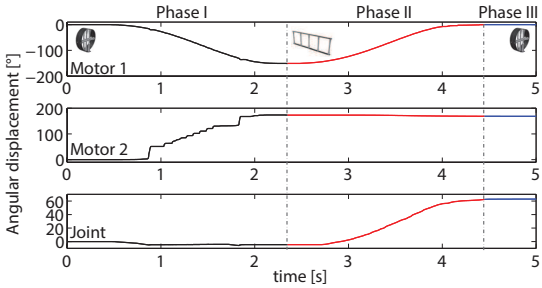

Fig. 12. Discrete motion application. Phase I: reconfiguration (in black), phase II motion application (in red), phase III all motors disabled (in blue).

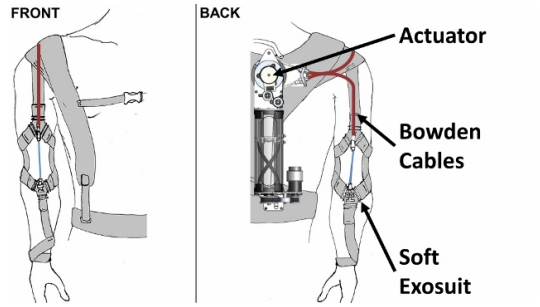

Fig. 13. Concept design of an exosuit comprising the actuator.

a relatively small hardware. The most novel features are the ability of the MCT to store and release elastic energy, resulting in a smart series elastic element, and its non-linear transmission ratio. Such transmission however needs to be properly tuned: its properties strictly depend on the design parameters of the carbon fibre plies as described in previous works and the optimal combination requires design iterations. The resulting passive stiffness at the joint level should be increased so that the system would be able to passively sustain high loads for wider twisting angle range. Furthermore, the backlash introduced by the NBM affects widely the control thus the mechanism will undergo a design refinement in order to reduce its magnitude. The discrete motion paradigm introduces a delay corresponding to the reconfiguration phase and studies on how to decrease such delay will be performed as well as studies of different motion paradigms. Finally, studies on control stability of the proposed actuator and on frequency response will be performed. An embodiment of the soft wearable exoskeleton meant to be powered by the proposed actuator is currently under development (figure 13). The frame is made of smart textiles able to sustain the users limb and it makes use of the kinematics of the joint rather than providing an articulated external frame. This results in a lightweight, highly biomimetic device. Such exosuit is intended to be used as an assistive device for upper limb medical conditions where recovery is not likely, e.g. neurological level of injuries [18], or as an augmenting device for particular work conditions where human presence is not replaceable but physically demanding, e.g. production and assembly lines [19].

REFERENCES

[1] Dellon, B., & Matsuoka, Y. (2007). Prosthetics, exoskeletons, and rehabilitation. IEEE Robotics and Automation magazine, 14(1), 30.

[2] [2] Garcia, E., Sater, J. M., & Main, J. (2002). Exoskeletons for Human Performance Augmentation (EHPA): A Program Summary. Journal of the Robotics Society of Japan, 20(8), 822-826.

[3] Lo, H. S., & Xie, S. Q. (2012). Exoskeleton robots for upper-limb rehabilitation: State of the art and future prospects. Medical engineering & physics, 34(3), 261-268.

[4] Herr, H. (2009). Exoskeletons and orthoses: classification, design challenges and future directions. Journal of neuroengineering and rehabilitation, 6, 21

[5] Brackbill, E. A., Mao, Y., Agrawal, S. K., Annapragada, M., & Dubey, V. N. (2009). Dynamics and control of a 4-dof wearable cable-driven upper arm exoskeleton. In Robotics and Automation, 2009. ICRA'09. IEEE International Conference on (pp. 2300-2305). IEEE.

[6] Noda, T., Teramae, T., Ugurlu, B., & Morimoto, J. (2014, September). Development of an upper limb exoskeleton powered via pneumatic electric hybrid actuators with bowden cable. In Intelligent Robots and Systems (IROS 2014), 2014 IEEE/RSJ International Conference on (pp. 3573-3578). IEEE. Chicago

[7] Asbeck, A., De Rossi, S., Galiana, I., Ding, Y., & Walsh, C. (2014). Stronger, Smarter, Softer: Next-Generation Wearable Robots. Robotics & Automation Magazine, IEEE, 21(4), 22-33

[8] Lachenal, X., Weaver, P. M., & Daynes, S. (2012). Multi-stable composite twisting structure for morphing applications. Proceedings of the Royal Society A: Mathematical, Physical and Engineering Science, 468(2141), 1230-1251.

[9] Masia, L., Cappello, L., Morasso, P., Lachenal, X., Pirrera, A., Weaver, P., & Mattioni, F. (2013). CARAPACE: A novel composite advanced robotic actuator powering assistive compliant exoskeleton preliminary design. In Rehabilitation Robotics (ICORR), 2013 IEEE International Conference on (pp. 1-8). IEEE.

[10] Cappello, L., Lachenal, X., Pirrera, A., Mattioni, F., Weaver, P. M., & Masia, L. (2014). Design, characterization and stability test of a multistable composite compliant actuator for exoskeletons. In Biomedical Robotics and Biomechatronics (2014 5th IEEE RAS & EMBS International Conference on (pp. 1051-1056). IEEE.

[11] Ding, Y., Galiana, I., Asbeck, A., Quinlivan, B., De Rossi, S. M. M., & Walsh, C. (2014, May). Multi-joint actuation platform for lower extremity soft exosuits. In Robotics and Automation (ICRA), 2014 IEEE International Conference On (pp. 1327-1334). IEEE.

[12] Dempster, W. T., & Gaughran, G. R. (1967). Properties of body segments based on size and weight. American journal of anatomy, 120(1), 33-54.

[13] Pratt, G. A., & Williamson, M. M. (1995, August). Series elastic actuators. In Intelligent Robots and Systems 95.'Human Robot Interaction and Cooperative Robots', Proceedings. 1995 IEEE/RSJ International Conference on (Vol. 1, pp. 399-406). IEEE.

[14] Lens, T., & Von Stryk, O. (2012, October). Investigation of safety in human-robot-interaction for a series elastic, tendon-driven robot arm. In Intelligent Robots and Systems (IROS), 2012 IEEE/RSJ International Conference on (pp. 4309-4314). IEEE.

[15] Controzzi, M., Cipriani, C., & Carrozza, M. C. (2010). Miniaturized non-back-drivable mechanism for robotic applications. Mechanism and Machine Theory, 45(10), 1395-1406.

[16] Hogan, N. (1984). An organizing principle for a class of voluntary movements. The Journal of Neuroscience, 4(11), 2745-2754.

[17] Shadmehr, Reza. The computational neurobiology of reaching and pointing: a foundation for motor learning. MIT press, 2005.

[18] Kirshblum, S. C., Burns, S. P., Biering-Sorensen, F., Donovan, W., Graves, D. E., Jha, A. & Waring, W. (2011). International standards for neurological classification of spinal cord injury (revised 2011). The journal of spinal cord medicine, 34(6), 535-546.

[19] Airbus Group - Factory of the future. Exoskeletons for assembly, [Online] 2014, http://www.airbusgroup.com/int/en/story-overview/factory-of-the-future.html (Accessed: 11 March 2015).